

Computational ablative thermal response analysis of carbon/phenolic composites for thermal protection system

Taehoon Park¹, Kang-Hyun Lee¹ and Gun Jin Yun^{*1,2}

¹Department of Aerospace Engineering, Seoul National University,
Gwanak-gu Gwanak-ro 1 Seoul 08826, South Korea

²Institute of Advanced Aerospace Technology, Seoul National University,
Gwanak-gu Gwanak-ro 1, Seoul 08826, South Korea

(Received July 14, 2021, Revised August 27, 2021, Accepted August 31, 2021)

Abstract. This study presents an efficient computational methodology to perform ablative thermal response analysis of carbon/phenolic composites by introducing a novel dual-domain technique for heat transfer and gas diffusion physics. Phenomena such as in-depth heat transfer, material decomposition (i.e. pyrolysis), in-depth gas diffusion, and surface recession required for ablation analysis of carbon/phenolic composites are simulated. The proposed method is verified with reference simulation test data from Ablation Workshop for a one-dimensional model under four different combinations with surface heat flux, temperature, pressure boundary conditions, and surface recession conditions verified. A two-dimensional ablation problem was also solved, showing its scalability. Temperatures, recession depth, depth of boundaries between layers, the mass flux of char, and pyrolysis gas are obtained and compared with the reference for all cases.

Keywords: charring ablation; carbon/phenolic composite; finite element analysis; thermal protection system

1. Introduction

Hypersonic and supersonic air vehicles experience aerodynamic heating while traveling at high speeds in the atmosphere. Due to the vehicle's speed, the air is compressed at the surface and generates heat. This heat raises the surface temperature of the vehicle even by thousands of Kelvin (Anderson 2006). In order to protect the vehicle from heat, the thermal protection system (TPS) has been utilized in the last few decades. Since the amount of the generated heat is different according to the vehicle's trajectory, it is critical to developing an appropriate TPS.

Various materials are used for the TPS, and the ablative TPS material is mainly used when a large heat flux occurs (e. g., space missions). For the ablative TPS material, polymer composites with phenolic resin are typically used. The Phenolic Integrated Carbon Ablator (PICA) (Natali *et al.* 2016, Tran *et al.* 1997) and AVCOAT (Linda n.d.) developed by NASA were used in actual space missions. In the ablative TPS materials, complex phenomena occur in a high-temperature environment. The polymer matrix is decomposed into carbon mass and gases when the

*Corresponding author, Professor, E-mail: gunjin.yun@snu.ac.kr

temperature rises, called pyrolysis. When the pyrolysis occurs, the polymer matrix in the solid-state turns into a carbon mass (char), and the remaining elements become gases. These gases escape the vehicle's surface and interfere with the heat transfer, which also aids the protection of the surface. Due to the pyrolysis, a char layer is formed on the outermost part of the aircraft surface. This layer is particularly vulnerable to oxidation and suffers from various thermomechanical damages such as sublimation, melting, and spallation. Given that the shape of the TPS changes during flight, changing the aerodynamic flow and aerothermal heating, it is critical to predicting the shape changes.

Many studies have been conducted since the 1960s to predict the ablation of TPS materials. The development of the Charring Material Ablation code (CMA) was begun based on the theory for the overall ablation phenomena such as the in-depth response of polymer composites, the chemically reacting flow boundary layer, and the interaction between solids and fluids (Moyer *et al.* 1968, Kendall 1968, Rindal 1968, Bartlett *et al.* 1968a, b, c). The theory developed at this time has been still used in many studies until recent years. The Fully Implicit Ablation and Thermal (FIAT) codes were subsequently developed, and a fully implicit scheme was applied to the CMA theory (Chen and Milos 1999). Since the CMA/FIAT codes were limited to 1D, TITAN (Chen and Milos 2001) and 3DFIAT (Chen and Milos 2018) were also developed for an extension to 2D and 3D problems. Many studies based on the CMA theory use the simplified assumption of gas diffusion inside materials. Besides, some researchers have attempted to develop an advanced simulation technique for gas diffusion. Porous material Analysis Toolbox based on OpenFOAM (PATO) can simulate the multi-dimensional gas movement within the porous material by applying Darcy's law, and the chemical interaction between gas and solid has also been applied (Lachaud *et al.* 2014). The analysis scheme also differs depending on the code. For instance, CMA uses the finite difference method (FDM). On the other hand, FIAT and PATO use the finite volume method (FVM). In particular, the finite element method (FEM) has recently attracted attention due to its advantages of high computation efficiency, flexibility, and ability to model complex shapes compared to other methods (Dec 2010, Dec 2013, Dec 2012, Risch 2017, Wang *et al.* 2019). In-house codes such as Charring Ablator Response (CHAR) (Amar *et al.* 2016) and Heat Transfer and Erosion Analysis (HERO) (Ewing and Pincock, 2017) were also developed based on the FEM. Wang *et al.* 2019 increased the code's versatility by implementing the complex ablation phenomenon to commercial finite element software such as ABAQUS (Wang *et al.* 2019, Wang *et al.* 2018, Wang and Pasilio 2018). They successfully implemented the complex theories into ABAQUS user subroutines and verified the proposed codes through experiments for one-dimensional cases (Wang *et al.* 2019). However, their code uses the simplified gas diffusion equation, which does not fully reflect its complex nature.

This study aims to develop a more efficient and advanced methodology to perform ablation analysis of carbon/phenolic composites in the ABAQUS environment. Based on the CMA theory, the gas diffusion using Darcy's law, which was not considered in previous studies using ABAQUS, has been implemented by a novel dual-domain system technique due to ordinary differential equations' similarity between the heat transfer and gas diffusion physics. The limitation of the ABAQUS, that two main physical phenomena (heat transfer and gas diffusion) cannot be analyzed simultaneously, is overcome by adopting the dual-domain system. The developed method is also verified for one-dimensional cases through tests provided by Ablation Workshop (Lachaud *et al.* 2011, Lachaud *et al.* 2012). Besides, by applying the developed method in a 2D problem, the accuracy in the multi-dimensional complex-shape model is also confirmed. Section 2 explains the fundamental theories related to the ablation of carbon/phenolic composites. Section 3 includes

applying the related theories to ABAQUS. Lastly, Section 4 includes the verification of the results. Conclusions are made in Section 5.

2. Basic governing equations

Various phenomena such as Fig. 1 occur in ablative TPS materials such as carbon/phenolic composite in an aerodynamic heating situation. The heat generated from compressed air near the vehicle's surface is transferred to the TPS through convection or radiation. The arrived heat is transferred into the material in the form of conduction and raises the temperature. Above a specific temperature, the polymer matrix is pyrolyzed and decomposed into a char layer and pyrolysis gas. Since this reaction is endothermic, it interferes with the heat transfer. As the heat transfer proceeds, the pyrolysis zone gradually propagates into the material, and the char layer deepens. The pyrolysis gas generated inside passes through the porous char layer and exits through the surface. The movement of these gases is also an essential factor that hinders heat transfer. The outermost shell of TPS is a char layer, and it is vulnerable to sublimation and spallation and chemical reactions such as oxidation, and the recession occurs. Many researchers have made mathematical derivations of these complex phenomena (Bartlett *et al.* 1968a, b, c Moyer *et al.* 1968, Kendall 1968, Rindal 1968, Dec 2010, Dec 2013). Next, each phenomenon's equations are primarily divided into four types: in-depth heat transfer, material decomposition, in-depth gas diffusion, and surface heat flux, and each of them will be explained in the following sections.

2.1 Surface heat flux

The surface energy balance equation can be derived from in and out energies for a control volume shown in Fig. 2.

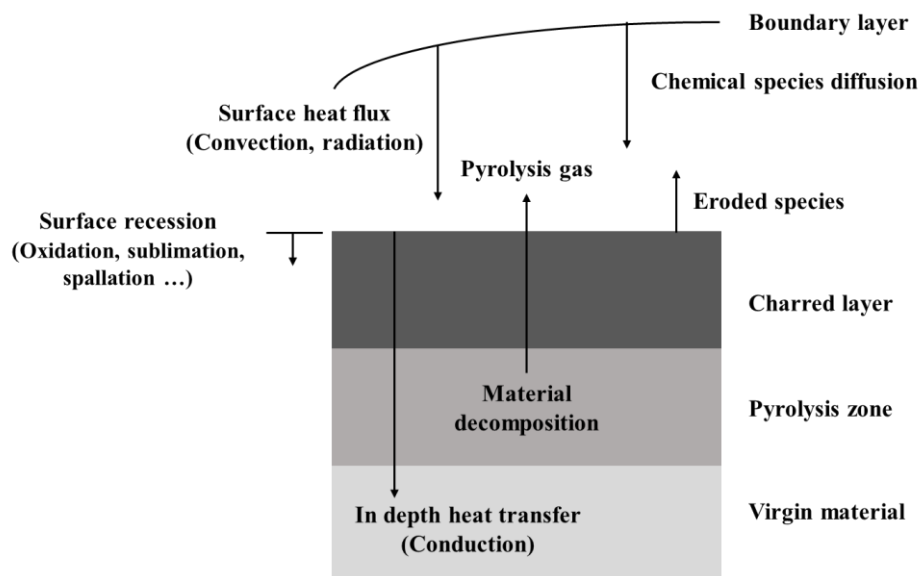


Fig. 1 Various phenomena occurring during ablation of carbon/phenolic composite

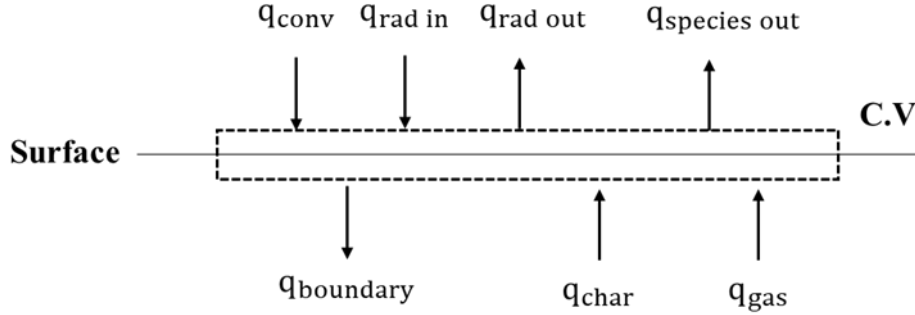


Fig. 2 Energy balance at the surface (C.V: Control Volume)

$$q_{boundary} = \rho_e U_e C_H (\dot{h}_r - \dot{h}_w) + \rho_e U_e C_H (B'_c \dot{h}_c + B'_g \dot{h}_g - B' \dot{h}_w) - \sigma \varepsilon (T_w^4 - T_\infty^4) \quad (1)$$

where ρ_e and U_e denote the density and velocity of flow at the edge of the boundary layer, respectively. h_r is the recovery enthalpy, h_w is the enthalpy on the surface. C_H is the Stanton number. On the outermost surface of the TPS, various phenomena such as energy flow and chemical reaction occur. As shown in Fig. 2, various heat types affect the TPS surface, and the relationship between the heats can be defined using the energy balance (Eq. (1)). The heat transferred to the inside of the TPS ($q_{boundary}$) can be obtained through the external convective heat flux entering into the material ($\rho_e U_e C_H (h_r - h_w)$), the energy of the materials leaving the TPS surface ($\rho_e U_e C_H (B'_c h_c + B'_g h_g - B' h_w)$), and the net radiative heat flux ($\sigma \varepsilon (T_w^4 - T_\infty^4)$). The species flux leaving the surface can be obtained as the sum of the pyrolysis gas flux and the char flux as in Eq. (2)

$$q_{boundary} = \rho_e U_e C_H (\dot{h}_r - \dot{h}_w) + \rho_e U_e C_H (B'_c \dot{h}_c + B'_g \dot{h}_g - B' \dot{h}_w) - \sigma \varepsilon (T_w^4 - T_\infty^4) \quad (1)$$

$$(\rho u)_w = \dot{m}_g'' + \dot{m}_c'' \quad (2)$$

$$B' = \frac{(\rho u)_w}{\rho_e U_e C_H}, \quad B'_g = \frac{\dot{m}_g''}{\rho_e U_e C_H}, \quad B'_c = \frac{\dot{m}_c''}{\rho_e U_e C_H} \quad (3)$$

B' values are non-dimensional ablation rates obtained by dividing the mass flux of the material exiting the TPS by the convective heat transfer coefficient ($\rho_e U_e C_H$) (Eq. (2)-Eq. (3)). \dot{m}_c'' represents the amount of erosion of the outermost char layer of the TPS and dividing this by the density gives the surface recession rate.

$$\dot{s} = \frac{\dot{m}_c''}{\rho_c} \quad (4)$$

Besides, the Stanton number (C_H) decreases by the species exiting the surface, which is called the blowing effect and is expressed as Eq. (5), and λ is 0.5 in this work (Moyer and Rindal 1968).

$$\frac{C_H}{C_{H0}} = \frac{\ln(1 + 2\lambda B)}{2\lambda B} \quad (5)$$

where C_H is the corrected Stanton number and C_{H0} is the original Stanton number.

2.2 In-depth heat transfer

The governing equation for heat transfer with pyrolyzing is shown in Eq. (6) (Dec 2010). The left side is a term for the internal energy of solid material. The first term on the right side relates to heat conduction, the second term is the heat absorbed by pyrolysis, the third term relates to the effect of the recession, and the fourth term relates to the movement of the pyrolysis gas.

$$\rho C_p \frac{\partial T}{\partial t} = \nabla \cdot (k \nabla T) + (\dot{h}_g - \bar{h}) \frac{\partial \rho}{\partial t} + \dot{s} \rho C_p \nabla T + \dot{m}_g'' C_{pg} \nabla T \quad (6)$$

Here, ρ is current density, C_p is heat capacity, k is the conductivity of the solid material. \dot{h}_g and C_{pg} denote the enthalpy and heat capacity of the pyrolysis gas, respectively. \bar{h} is the mass-weighted average enthalpy of the virgin and char materials and can be obtained as follows.

$$\bar{h} = \frac{\rho_v h_v - \rho_c h_c}{\rho_v - \rho_c} \quad (7)$$

2.3 Material decomposition



The elevated temperature decomposes polymeric materials such as phenolic resin. When the polymer virgin material is pyrolyzed, char consisting of carbon is produced, and the remaining elements are discharged in the form of gas (Eq. (8)). As the gas exits the material, the material becomes porous, and its density decreases. The density of carbon/phenolic composite changes non-linearly with the current temperature and density, as shown in Eq. (9) (Goldstein 1969).

$$\frac{\partial \rho_i}{\partial t} = -A_i \exp\left(-\frac{E_i}{RT}\right) \rho_{v,i} \left(\frac{\rho_i - \rho_{c,i}}{\rho_{v,i}}\right)^{\psi_i} \quad (i = A, B, C) \quad (9)$$

where A_i is the pre-exponential factor, E_i is the activation energy, R is the gas constant, T is the temperature, ρ_i is the current density, $\rho_{c,i}$ is the char density, $\rho_{v,i}$ is the virgin material density, and ψ_i is the reaction order. This study assumes that it comprises three substances A, B, and C, with different pyrolysis properties for the simulation of complex polymer pyrolysis. A and B are the polymer material with different decomposition kinetics and C is the fiber. By independently calculating the decomposition of A and B, a complex two-step pyrolysis phenomenon can be modeled. The density of the solid composite material can be obtained through the density and volume fraction (Γ) of the three materials as follows.

$$\rho = \Gamma(\rho_A + \rho_B) + (1 - \Gamma)\rho_C \quad (10)$$

The degree of decomposition can be obtained from the current density, the density of virgin material, and the char density as Eq. (11). Using the degree of decomposition, the properties of the material undergoing pyrolysis can be computed assuming that the thermal properties linearly vary with local volume fractions of charred materials as Eq (12)-(14)

$$\tau = \frac{1 - \frac{\rho_c}{\rho}}{1 - \frac{\rho_c}{\rho_v}} \quad (11)$$

$$C_p = \tau C_{p,v} + (1 - \tau)C_{p,c} \quad (12)$$

$$k = \tau k_v + (1 - \tau)k_c \quad (13)$$

$$\kappa = \tau \kappa_v + (1 - \tau)\kappa_c \quad (14)$$

2.4 In-depth gas diffusion

As mentioned earlier, when the solid material is pyrolyzed, its density decreases with the generation of gas. Supposing that no chemical reaction takes place between the gas and the solid material (the gas also escapes from the solid material as soon as it is created), the gas is generated by the amount by which the density of the solid material decreases. Then, an equation can be derived as follows (Dec 2010).

$$\nabla \cdot \dot{m}_g'' = \frac{\partial \rho}{\partial t} \quad (15)$$

The pyrolysis gas movement is shown in Eq. (16) using Darcy's law, a law for fluid passing through the porous material.

$$\dot{m}_g'' = -\frac{\rho_g \kappa}{\mu \phi} \nabla P \quad (16)$$

where μ and ϕ are the viscosity and porosity, respectively; P is the pressure; and κ is the permeability. Through Eq. (15) and Eq. (16), the final equation for gas generation and diffusion can be obtained as follows.

$$\frac{\partial \rho}{\partial t} + \nabla \cdot \left(\frac{\rho_g \kappa}{\mu \phi} \nabla P \right) = 0 \quad (17)$$

3. Methodology

The developed method of ablation analysis using ABAQUS is as shown in Fig. 3. When the various equations discussed in Section 2 are implemented to ABAQUS with the modeled thermal material behavior, ABAQUS performs ablation analysis and derives analysis results such as temperature, pressure, and density fields to the users. All equations must be appropriately applied to ABAQUS to ensure convergence and proper material properties must be considered for accurate

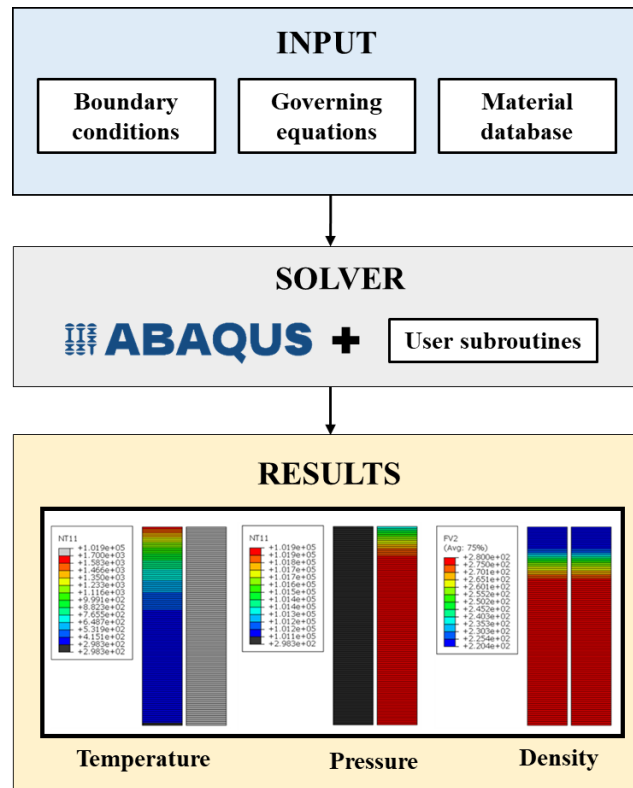


Fig. 3 Framework of ablation analysis using ABAQUS

interpretation. Equations related to the ablation of carbon/phenolic composites are implemented to ABAQUS using its provided user subroutine. In particular, the material properties are taken from the open-source database, TACOT.

3.1 ABAQUS user subroutines

In ABAQUS, users can implement boundary conditions and material modeling in various situations using user subroutines written in the Fortran language. Various physical phenomena introduced in Chapter II are applied to ABAQUS using several subroutines, as shown in Fig. 4. UEXTERNALDB is used to read the external data such as boundary conditions as well as the varying material properties, and to store the output field values such as temperature and density. USDFLD is used to implement the material decomposition. It is called at all integration points and calculates the current density by solving Eq. (9) explicitly. Then, the corresponding material properties at each integration point are also obtained using Eq. (11)-(14). With material properties computed in USDFLD, UMATHT defines material behaviors with in-depth heat transfer (Eq. (6)) and gas diffusion (Eq. (17)). Here, the heat transfer and the gas diffusion were simultaneously applied using a dual-domain system, which will be discussed later. DISP is used to define the pressure boundary condition, which is used for the gas diffusion analysis. With DFLUX, the heat flux boundary condition (Eq. (1)) is applied to the desired position. After all boundary conditions and governing equations have been implemented, ABAQUS derives the solutions (temperature and

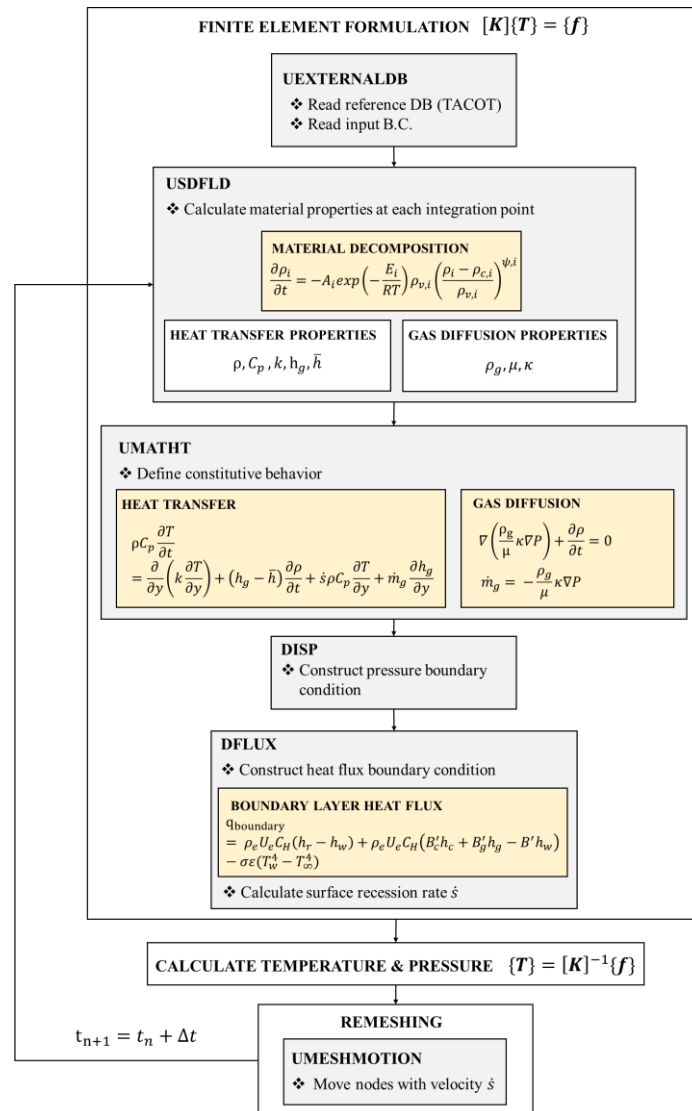


Fig. 4 Procedure for ablation analysis of carbon/phenolic composites using ABAQUS

pressure). After the temperature and pressure fields are computed, UMESHMOTION calculates the erosion rate (Eq. (4)) and moves the surface node. The mesh is then refined using arbitrary Lagrangian-Eulerian (ALE) method, and the solution variable is re-mapped to the new mesh. The above procedures are repeated until the last analysis step is completed.

3.2 Dual-domain system

Although ABAQUS provides some frameworks to perform various multiphysics analysis (Lin and Lafarie-Frenot 2018, Ghashochi-Bargh *et al.* 2020, Lee and Yun 2021), heat transfer and gas diffusion cannot be analyzed simultaneously in the ABAQUS. It is the dual-domain system that

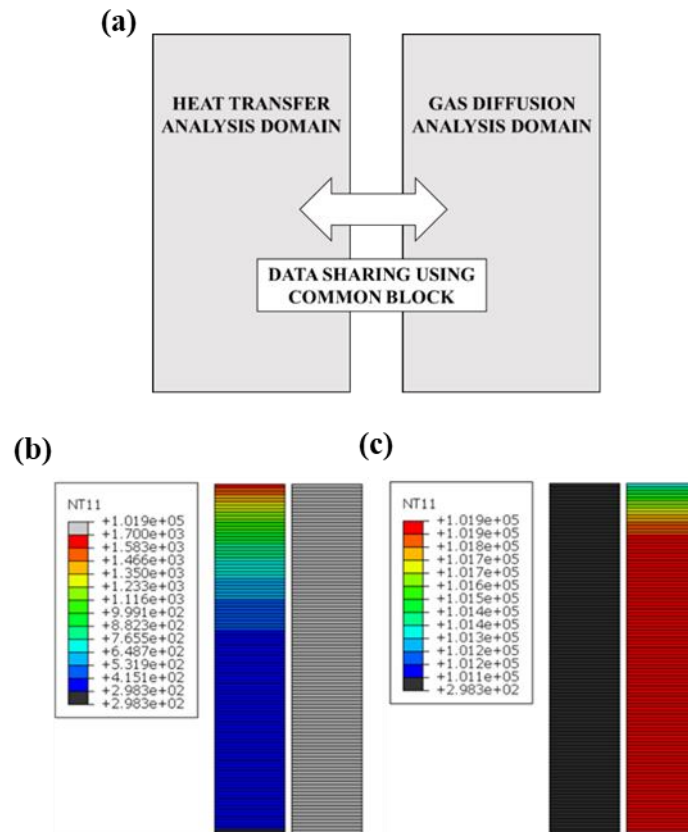


Fig. 5 (a) Schematic of the dual-domain system and the ABAQUS visualization of (b) temperature and (c) pressure obtained using dual-domain system

makes this possible. In-depth heat transfer equation (Eq. (6)) and gas diffusion equation (Eq. (17)) have a similar form as both equations have time derivatives and Laplacian terms. Originally, UMATHT is a subroutine for definition of material behavior in heat transfer analysis. However, the gas diffusion can also be analyzed using the similarity of the two equations (Eq. (6) and (17)). Assuming the pressure as an imaginary temperature and applying material properties for pressure analysis instead of thermal analysis into UMATHT, ABAQUS can perform the gas diffusion analysis. However, since UMATHT is called only once at one integration point, one domain is divided into two virtual domains to perform heat transfer analysis and gas diffusion analysis simultaneously as shown in Fig. 5. As can be seen in Fig. 5(b) and 5(c), where the contours of the nodal temperature in both domains are viewed, temperature values are shown in the heat transfer analysis domain and pressure values are shown in the gas diffusion domain. In order to effectively visualize temperature and pressure fields, the range of the nodal temperature values is adjusted in each case. For cases where analysis results in one domain are needed for another analysis domain (such as decomposition rate ($\frac{\partial \rho}{\partial t}$) and mass flux (\dot{m}_g'')), values are shared through a common block provided by Fortran. In addition, there are studies that have analyzed various physical phenomena using a dual-domain system (Lee and Kannatey-Asibu 2009, Li *et al.* 2020).

3.3 Theoretical ablative composite for open testing (TACOT)

Basic properties required for analysis are taken from the TACOT database (Van Eekelen *et al.* 2012). TACOT is an open-source database released for verification of ablation analysis of carbon/phenolic composite. Structural properties (volume fraction, porosity, permeability), thermal properties (heat capacity, thermal conductivity, enthalpy), pyrolysis gas properties (molar mass, heat capacity, enthalpy, viscosity, density), parameters about pyrolysis, and B' table for recession and heat flux boundary conditions are included in this database.

4. Results

In order to verify the proposed analysis method, the ablation workshop's test cases are used (Lachaud *et al.* 2011, Lachaud *et al.* 2012). There are four test cases for a one-dimensional model and one test case for a two-dimensional model. Various situations are designed by changing the boundary conditions. A brief description of each case for the one-dimensional model can be found in Table 1. The initial condition and boundary condition are shown in Fig. 6. In Case 1, only temperature and pressure boundary conditions are applied to the top surface without surface heat flux boundary conditions and recession. In case 2, the heat flux boundary condition is applied to the top surface, and recession is not considered. Cases 3 and 4 consider recession in the heat flux boundary condition, but the magnitudes of the heat flux are different. In Cases 2, 3 and 4, heat flux boundary conditions that change over time are applied as shown in Fig. 7. The analysis is performed for 60 seconds in Case 1 and 120 seconds for Case 2, 3, and 4. Detailed values of the boundary conditions are shown in Table 2.

Table 1 Summary of test case

Test case	Description
1	No surface heat flux boundary condition, constant temperature boundary condition, constant pressure boundary condition, no recession
2	Low surface heat flux boundary condition, no temperature boundary condition, constant pressure boundary condition, no recession
3	Low surface heat flux boundary condition, no temperature boundary condition, constant pressure boundary condition, recession
4	High surface heat flux boundary condition, no temperature boundary condition, constant pressure boundary condition, recession

Table 2 Boundary condition values

Test case	Temperature B.C. (K)	Pressure B.C. (Pa)	$\rho_e U_e C_H \max$ ($\text{kg} \cdot \text{m}^{-2} \cdot \text{s}^{-1}$)	$h_r \max$ ($\text{J} \cdot \text{kg}^{-1}$)
1	1644	101325	X	X
2	X	101325	0.3	$1.5 \cdot 10^6$
3	X	101325	0.3	$1.5 \cdot 10^6$
4	X	101325	0.3	$2.5 \cdot 10^7$

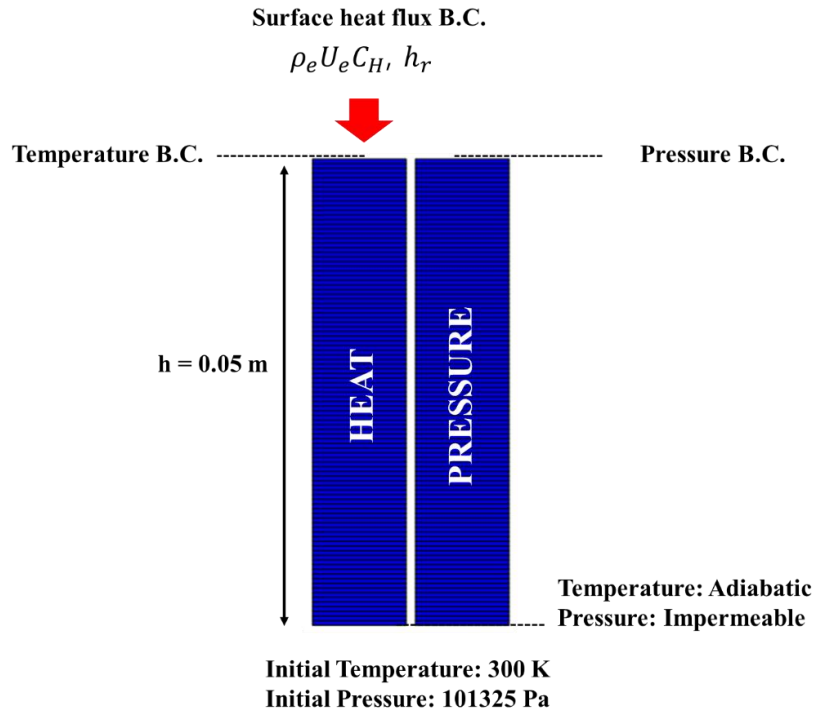


Fig. 6 Geometry and boundary conditions of the analysis model

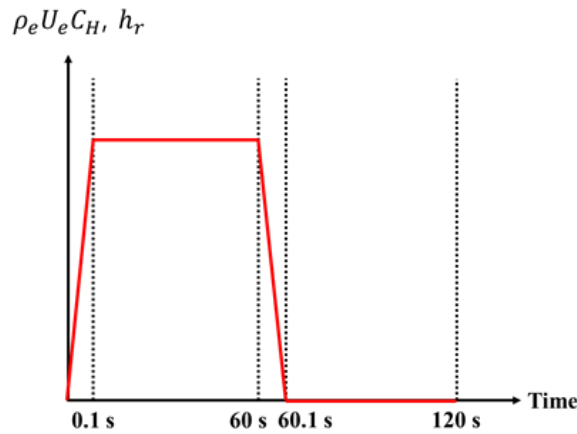


Fig. 7 Heat flux boundary conditions that change with time

Each case is verified by three types of data: the first type is the in-depth temperature reaction, the second type is the in-depth pyrolysis response, and the third type is the surface recession response. In the case of the in-depth temperature reaction, the result is obtained by measuring the temperature change over time at 10 probe points (top surface, 1 mm, 2 mm, 4 mm, 8 mm, 12 mm, 16 mm, 24 mm, 50 mm from the initial surface) (Fig. 8 (a)). The top surface probe is a Lagrangian

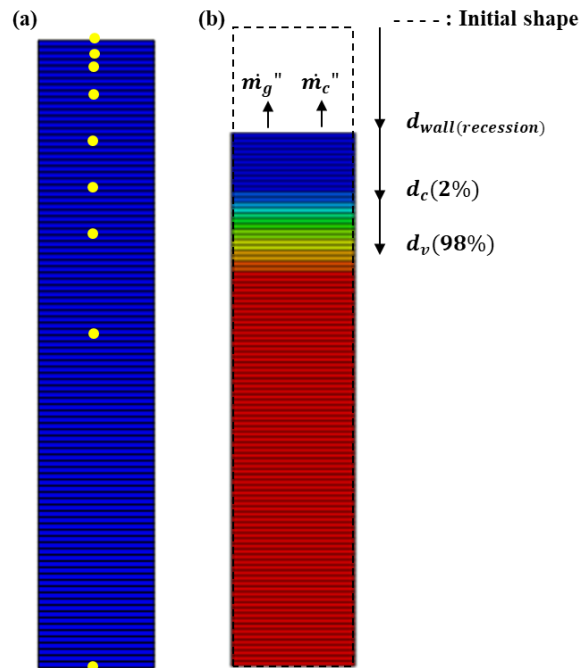


Fig. 8 Three types of output data. (a) Thermal response probe points and (b) pyrolysis and recession response (blue: charred layer, green: pyrolysis zone, red: virgin layer)

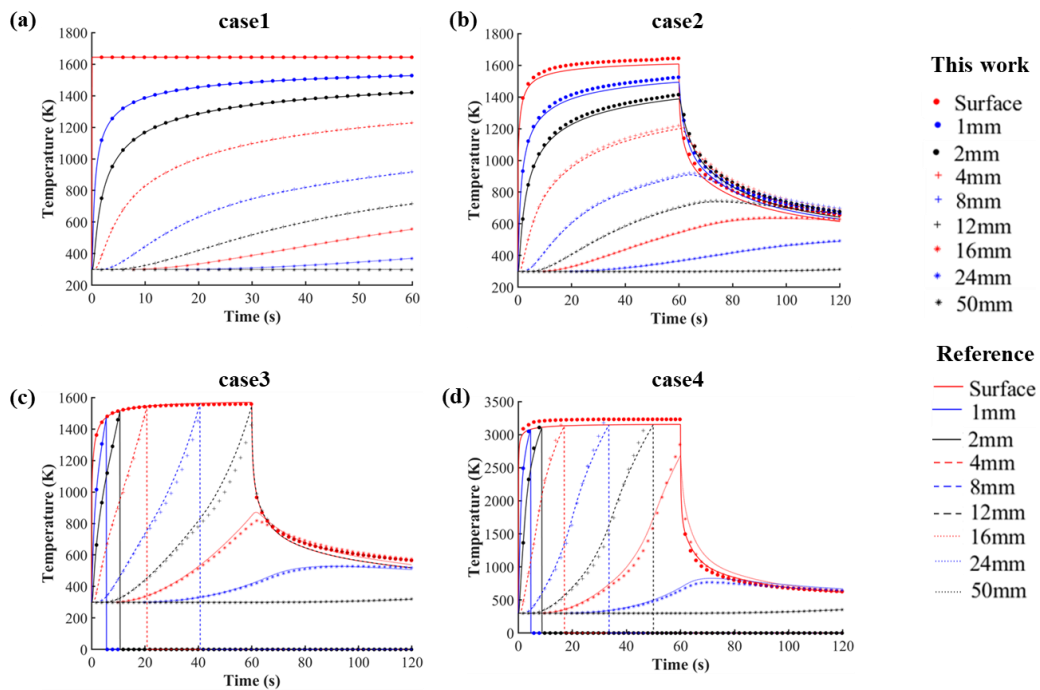


Fig. 9 Thermal response data from Case 1-4. Reference data from (Lachaud *et al.* 2011, Lachaud *et al.* 2012)

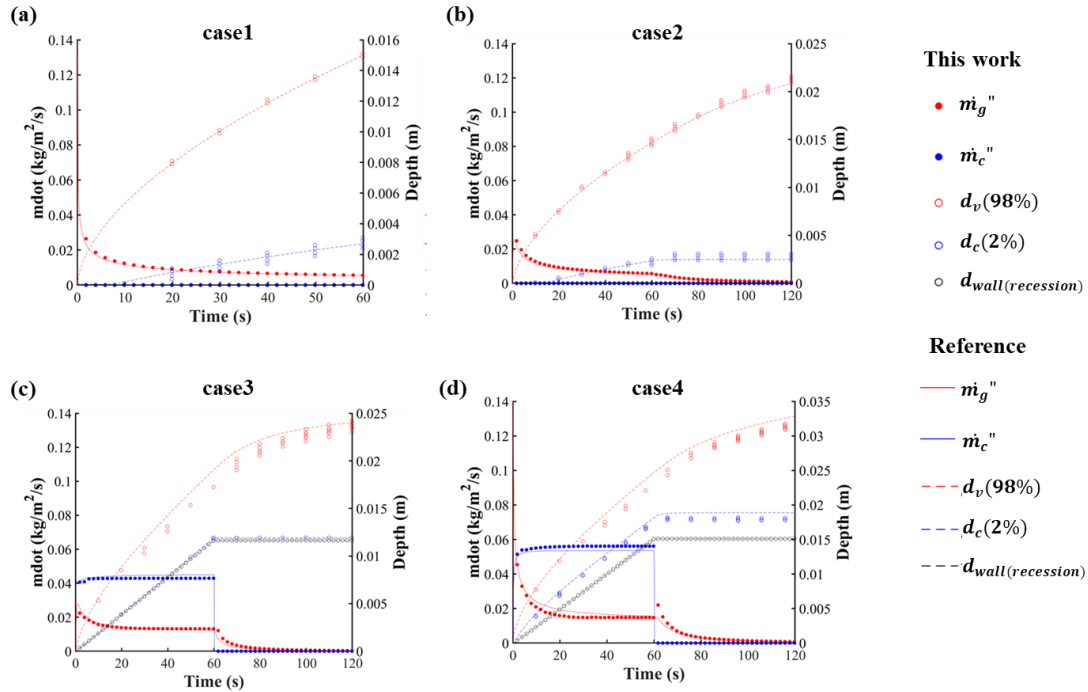


Fig. 10 In-depth pyrolysis and surface recession response data of Case 1-4. Reference data from (Lachaud *et al.* 2011, Lachud *et al.* 2012)

point that moves along the recession surface and the remaining points are Eulerian (which are fixed at their initial position). The temperature at a fixed point is obtained by interpolation of the temperatures at integral points of the element containing the corresponding point. In the case of in-depth pyrolysis, the boundary between the charred layer and the pyrolysis zone (d_c (2%)), the boundary between the pyrolysis zone and the virgin layer (d_v (98%)), and the amount of pyrolysis gas generated by pyrolysis leaving the surface (\dot{m}_g'') are used (Fig. 8(b)) to verify the result. Depth of boundaries (d_c, d_v) are determined by the degree of decomposition (Eq. (11)) calculated in USDFLD. Also, \dot{m}_g'' is obtained using the pressure gradient (Eq. (16)) calculated in the pressure domain of UMATHHT. Unlike in-depth, moving velocity of the node on the surface where the erosion occurred is significant. Therefore, \dot{m}_g'' is corrected ($\dot{m}_g = \dot{m}_g - |\dot{S}| \times (\rho_{virgin} - \rho_{char})$) considering the velocity of the node. The surface recession response can be verified using wall (recession) depth and the amount of char leaving the surface (\dot{m}_c'') (Fig. 8(b)).

Fig. 9 shows the temperature change over time at the ten probe points. In all cases, it is consistent with the results of the reference, which means that the model proposed in this study accurately simulates the in-depth heat transfer of carbon/phenolic composites in various situations such as heating, cooling, and recession of surface. Fig. 10 shows the in-depth pyrolysis response data and the surface recession data. The boundaries d_c and d_v show that the current model properly simulates the material decomposition phenomenon. Furthermore, \dot{m}_g shows that dual-domain system applied in this study can predict the pyrolysis gas movement. d_{wall} shows that the surface recession modeling using UMESHMOTION works well.

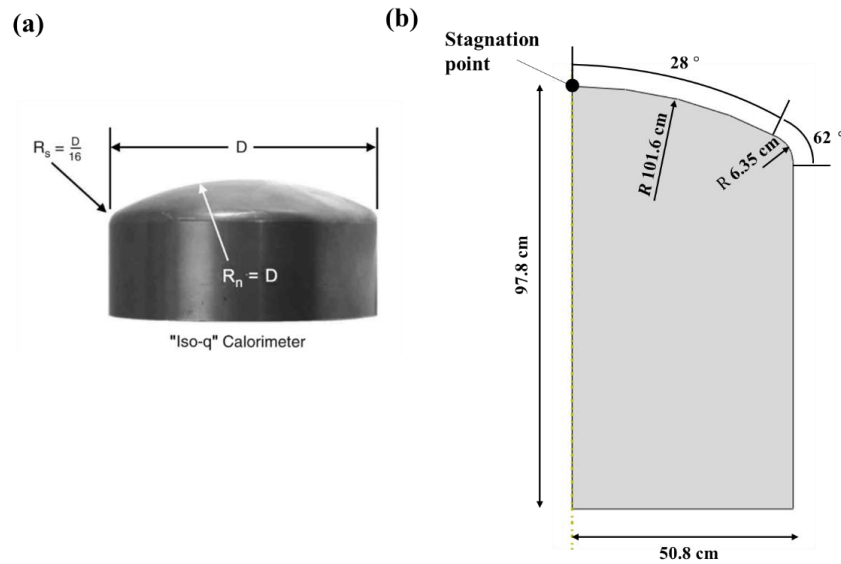


Fig. 11 (a) The actual specimen used in the arcjet test (Chen and Milos 2001) and (b) a model based on it

Table 3 Boundary condition values at stagnation point over time

Time (s)	$\rho_e U_e C_H$ ($\text{kg} \cdot \text{m}^{-2} \cdot \text{s}^{-1}$)	h_r ($\text{J} \cdot \text{kg}^{-1}$)	p_w (Pa)
0	0	0	101325
0.1	0.3	$2.5 \cdot 10^7$	101325
40	0.3	$2.5 \cdot 10^7$	101325
40.1	0	0	101325
120	0	0	101325

Table 4 Scale factor of heat flux boundary condition according to location

X	Y	q_w/q_{w0}	X	Y	q_w/q_{w0}
0.000	0.000	1	5.068	1.617	0.476
1.987	0.196	1	5.080	1.864	0.261
2.957	0.439	0.971	5.080	2.114	0.169
3.431	0.597	0.955	5.080	2.614	0.137
3.898	0.777	0.925	5.080	4.114	0.111
4.354	0.980	0.863	5.080	6.114	0.101
4.800	1.209	0.743	5.080	9.780	0.101

The proposed method is also applied to an axis-symmetric 2D model such as Fig. 11 to confirm the scalability to multi-dimensional and complex shapes. In the case of 1D problem, the heat flux and pressure boundary conditions are applied only to the top surface (Fig. 6), whereas the boundary conditions are applied to the top round surface and sidewall in the case of a 2D problem. The rest of the initial and boundary conditions are the same as in the 1D cases. The heat flux and pressure boundary condition values overtime at the stagnation point are shown in Table 3. At

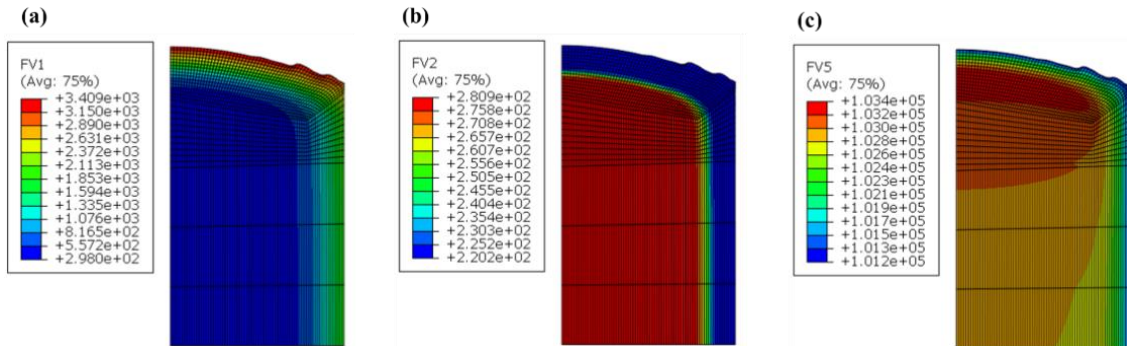


Fig. 12 (a) Temperature, (b) density, and (c) pressure contour after 40 s

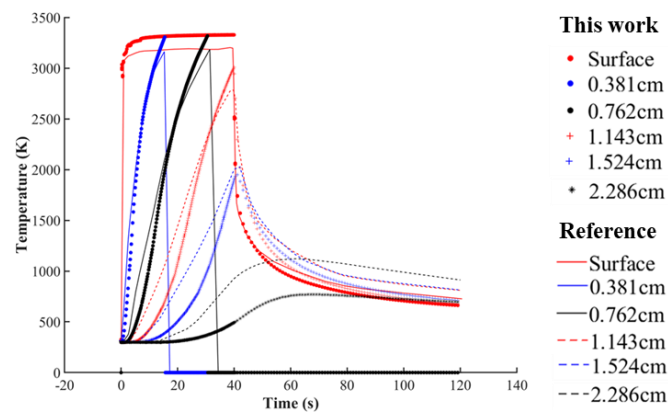


Fig. 13 Thermal response data from 2D case. Reference data from (Van Eekelen *et al.* 2012)

positions other than the stagnation point, the heat flux changes depending on the position by multiplying the scale factor (q_w/q_{w0} , q_w : corrected heat flux, q_{w0} : original heat flux) of Table 4 by the coefficient ($\rho_e U_e C_H$). In Table 4, the origin of X and Y coordinates (X=0, Y=0) is the stagnation point. Further information about 2D modeling can be found in (Chen and Milos 2001, Van Eekelen *et al.* 2012).

Fig. 12 shows the temperature, density, and pressure contours at 40s. It can be seen that the current method simulates in-depth heat transfer, density change according to material decomposition, and pressure change due to the generation of pyrolysis gas in 2D case. Fig. 13 shows the thermal response data of the 2D case. The result shows that there are discrepancies between the reference and this work. Furthermore, the differences increase as the depth increases. It can be said that the discrepancies are caused by various reasons such as differences in numerical analysis schemes or differences in the custom-written code compared to the commercial software.

5. Conclusions

In this paper, ablation theory and an efficient computational simulation methodology are presented that can simulate the ablative thermal response of carbon/phenolic composites, a representative material used in heat shielding structures. The method was constructed in

ABAQUS, a commercial finite element analysis software. Theoretical equations for various phenomena occurring in ablation, such as surface heat flux, in-depth heat transfer, material decomposition, and in-depth gas diffusion, were discussed and converted to be applicable to ABAQUS using various user subroutines, including USDFLD, UMATHT, DFLUX, and UMESHMOTION. The authors also tried to analyze the motion of pyrolysis gas with the implementation of the dual-domain system using the similarity between the heat transfer equation and the gas diffusion equation so that both simulations can be performed simultaneously. The developed method was also verified using the test cases of various boundary conditions provided by the Ablation Workshop. For material properties, an open-source database TACOT was used. In order to validate the proposed method, the analysis results, including temperatures, recession depth, depth of boundaries between layers, the mass flux of char, and pyrolysis gas, were obtained and compared with the reference for a total of four cases. It was found that the analysis results from the proposed method are consistent with the reference. The proposed method was also applied to a 2D model for verification in a multi-dimensional problem. Therefore, we conclude that the developed methodology can perform ablation analysis of phenolic composites.

The advantage of the current method is that ABAQUS, a versatile commercial program that can use various functions, is used. It is easy to add new functions based on current research. In the future, research will be conducted on the addition of new phenomena such as coking that are not currently considered, expansion to complex shapes, multi-physics analysis such as linkage with CFD, and application of multi-scale analysis using molecular dynamics.

Acknowledgments

This work was supported by the Creative-Pioneering Researchers Program, the Institute of Engineering Research at Seoul National University, and the BK21 Program funded by the Ministry of Education (MOE, Korea) and National Research Foundation of Korea. The authors are grateful for their supports.

References

- Amar, A.J., Brandon Oliver, A., Kirk, B.S., Salazer, G. and Droba, J (2016), "Overview of the charring ablator response (CHAR) code", *Proceedings of the 46th AIAA Thermophysics Conference*, Washington, D.C., U.S.A., June.
- Anderson, J.D. (2006), "Hypersonic and high-temperature gas dynamics", American Institute of Aeronautics and Astronautics
- Barlett, E.P., Kendall, R.M. and Rindal, R.A (1968), "An analysis of the coupled chemically reacting boundary layer and charring ablator. Part 4-A unified approximation for mixture transport properties for multicomponent boundary-layer applications", NASA Contractor Report.
- Bartlett, E.P. and Kendall, R.M. (1968), "An analysis of the coupled chemically reacting boundary layer and charring ablator. part 3-nonsimilar solution of the multicomponent laminar boundary layer by an integral matrix method", NASA Contractor Report.
- Bartlett, E.P., Kendall, R.M., Moyer, C.B. and Rindal, R.A (1968), "An analysis of the coupled chemically reacting boundary layer and charring ablator, Part 1 Summary report", NASA Contractor Report.
- Chen, Y.K. and Milos, F.S (1999), "Ablation and thermal response program for spacecraft heatshield analysis", *J. Spacecraft Rockets*, **36**, 475-483. <https://doi.org/10.2514/2.3469>.
- Chen, Y.K. and Milos, F.S (2001), "Two-dimensional implicit thermal response and ablation program for charring materials", *J. Spacecraft Rockets*, **38**, 473-481. <https://doi.org/10.2514/2.3724>.

- Chen, Y.K. and Milos, F.S (2018), "Multidimensional finite volume fully implicit ablation and thermal response code", *J. Spacecraft Rockets*, **55**, 914-927. <https://doi.org/10.2514/1.A34184>.
- Dec, J.A (2010), "Three dimensional finite element ablative thermal response analysis applied to heatshield penetration design", Ph.D Thesis, Georgia Institute of Technology, Georgia, Atlanta, U.S.A.
- Dec, J.A. and Braun, R.D (2013), "Three-dimensional finite element ablative thermal response and design of thermal protection systems", *J. Spacecraft Rockets*, **50**, 725-734. <https://doi.org/10.2514/1.A32313>.
- Dec, J.A. and Braun, R.D (2012), "Ablative thermal response analysis using the finite element method", *J. Thermophys. Heat Transf.*, **26**, 201-212. <https://doi.org/10.2514/1.T3694>.
- Ewing, M.E. and Pincock, B (2017), "Heat transfer modeling of a charring material using isoconversional kinetics", *Heat Transfer Eng.*, **38**, 1189-1197. <https://doi.org/10.1080/01457632.2016.1239939>.
- Ghashochi-Bargh, H., Goodarzi, M.S., Karimi, M. and Salamat-Talab, M. (2020), "Transient thermoelastic analysis of carbon/carbon composite multidisc brake using finite element method", *Adv. Aircraft Spacecraft Sci.*, **7**(2), 135-149. <https://doi.org/10.12989/aas.2020.7.2.135>.
- Goldstein, H.E (1969), "Pyrolysis kinetics of nylon 6-6, phenolic resin, and their composites", *J. Macromol. Sci. Part A Chem.*, **3**, 649-673. <https://doi.org/10.1080/10601326908053834>.
- Kendall, R.M (1968), "An analysis of the coupled chemically reacting boundary layer and charring ablator. Part 5-A general approach to the thermochemical solution of mixed equilibrium-nonequilibrium, homogeneous or heterogeneous systems", NASA Contractor Report.
- Lachaud, J. and Mansour, N.N (2014), "Porous-material analysis toolbox based on openfoam and applications", *J. Thermophys. Heat Transf.*, **28**, 191-202. <https://doi.org/10.2514/1.T4262>.
- Lachaud, J.R., Martin, A., Van Eekelen, T. and Cozmuta, I (2012), "Ablation Test-Case Series #2", *Proceedings of the 5th Ablation Workshop*, Lexington, Kentucky, U.S.A., February-March.
- Lachaud, J., Laub, B., Martin, A. and Cozmuta, I (2011), "Ablation workshop test case", *Proceedings of the 4th Ablation Workshop*, Albuquerque, New Mexico, U.S.A., March.
- Lee, D. and Kannatey-Asibu, E (2009), "Numerical analysis of ultrashort pulse laser-material interaction using ABAQUS", *J. Manuf. Sci. Eng.*, **131**(2), 0210051-02100515. <https://doi.org/10.1115/1.3075869>.
- Lee, K.H. and Yun, G.J. (2021). "Temperature thread multiscale finite element simulation of selective laser melting for the evaluation of process", *Adv. Aircraft Spacecraft Sci.*, **8**(1), 31-51. <https://doi.org/10.12989/aas.2021.8.1.031>.
- Li, H., Fan, B., Wang, N., Han, X., Feng, Z. and Guo, S. (2020), "Thermal response study of carbon epoxy laminates exposed to fire", *Polym. Compos.*, 1-14. <https://doi.org/10.1002/pc.25750>.
- Lin, Y. and Lafarie-Frenot, M.C (2018), "Numerical simulation of the thermoelectric behavior of CNTs/CFRP aircraft composite laminates", *Adv. Aircraft Spacecraft Sci.*, **5**(6), 633-652. <http://doi.org/10.12989/aas.2018.5.6.633>.
- Linda, H (n.d.), "Heat shield install brings orion spacecraft closer to space", NASA's John F. Kennedy Space Center, <https://www.nasa.gov/feature/heat-shield-install-brings-orion-spacecraft-closer-to-space>.
- Moyer, C.B., and Rindal, R.A (1968), "An analysis of the coupled chemically reacting boundary layer and charring ablator. part 2-finite difference solution for the in-depth response of charring materials considering surface chemical and energy balances", NASA Contractor Report.
- Moyer, C.B. and Rindal, R.A (1968), "An analysis of the coupled chemically reacting boundary layer and charring ablator. part 2-finite difference solution for the in-depth response of charring materials considering surface chemical and energy balances", NASA CR-1061.
- Natali, M., Kenny, J.M. and Torre, L (2016), "Science and technology of polymeric ablative materials for thermal protection systems and propulsion devices: A review", *Prog. Mater. Sci.*, **84**, 192-275. <https://doi.org/10.1016/j.pmatsci.2016.08.003>.
- Rindal, R.A (1968), "An analysis of the coupled chemically reacting boundary layer and charring ablator. Part 6-An approach for characterizing charring ablator response with in-depth coking reactions", NASA Contractor Report.
- Risch, T.K (2017), "Verification of a finite element model for pyrolyzing ablative materials", *Proceedings of the 47th AIAA Thermophysics Conference*, Denver, Colorado, U.S.A., June.
- Tran, H.K., Johnson, C., Rasky, D., Hui, F., Hsu, M.T., Chen, T. and Kobayashi, L. (1997), "Phenolic

- impregnated carbon ablators pica as thermal protection system for discovery missions”, NASA TM-110440.
- Van Eekelen, T., Lachaud, J.R., Martin, A., and Cozmuta, I (2012), “Ablation Test-Case #3”, *Proceeding 5th Ablation Work*.
- Wang, Y. and Pasilio, C.L (2018), “Modeling ablation of laminated composites: A novel manual mesh moving finite element analysis procedure with ABAQUS”, *Int. J. Heat Mass Transf.*, 116, 306–313. <https://doi.org/10.1016/j.ijheatmasstransfer.2017.09.038>.
- Wang, Y., Risch, T.K. and Koo, J.H (2019), “Assessment of a one-dimensional finite element charring ablation material response model for phenolic-impregnated carbon ablator”, *Aerosp. Sci. Technol.*, **91**, 301-309. <https://doi.org/10.1016/j.ast.2019.05.039>.
- Wang, Y., Risch, T.K. and Pasilio, C.L (2018), “Modeling of pyrolyzing ablation problem with abaqus: A one-dimensional test case”, *J. Thermophys. Heat Transf.*, **32**, 542-545. <https://doi.org/10.2514/1.T5274>.

EC

Nomenclature

q	heat flux (W/m ²)
$\rho_e U_e C_H$	convective heat transfer coefficient (kg/m ² -s)
h	enthalpy (J/kg)
B'	non-dimensional ablation rate
\dot{m}''	mass flux (kg/m ² -s)
T	temperature (K)
σ	Stefan-Boltzmann constant (W/m ² -s-K ⁴)
ε	emissivity
\dot{s}	surface recession speed (m/s)
ρ	density (kg/m ³)
\bar{h}	mass weighted material enthalpy (J/kg)
A	pre-exponential factor (1/s)
E	activation energy (J/mol)
R	gas constant (8.314 J/(mol-K))
Γ	volume fraction

τ	degree of decomposition
C_p	heat capacity (J/kg-K)
k	thermal conductivity (W/m-K)
κ	permeability (m ²)
P	pressure (Pa)
μ	viscosity (Pa-s)
ϕ	porosity

Subscripts

e	freestream
c	char
v	virgin
g	gas
w	wall (surface)
r	recovery (boundary layer)

Appendix A. UMATHT Implementation

UMATHT is one of the most important subroutines in this analysis for in-depth heat transfer and gas diffusion analyses. In UMATHT, six values (Table A1) must be entered to obtain the Jacobian matrix of Eq. (A1). By adjusting these values, the users can model the desired phenomena.

$$J = \frac{1}{\Delta t} \int_V \delta T \rho \frac{\partial U}{\partial T} dT dV + \frac{1}{\Delta t} \int_V \delta T \rho \frac{\partial U}{\partial \mathbf{g}} \cdot d\mathbf{g} dV - \int_V \delta \mathbf{g} \cdot \frac{\partial \mathbf{f}}{\partial T} dT dV - \int_V \delta \mathbf{g} \cdot \frac{\partial \mathbf{f}}{\partial \mathbf{g}} \cdot d\mathbf{g} dV - \int_V \delta T \frac{\partial r}{\partial T} dT dV - \int_S \delta T \frac{\partial q}{\partial T} dT dS \quad (\text{A1})$$

The in-depth heat transfer equation such as Eq. (6) can be divided into two parts.

$$\dot{U} = \rho C_p \frac{\partial T}{\partial t} - (\dot{h}_g - \bar{h}) \frac{\partial \rho}{\partial t} - \dot{s} \rho C_p \nabla T - \dot{m}_g'' C_{pg} \nabla T \quad (\text{A2})$$

$$\mathbf{f} = -k \nabla T \quad (\text{A3})$$

Multiply both sides of Eq. (A2) by Δt and change it to the incremental form as shown below

$$\Delta U = \rho C_p \Delta T - (\dot{h}_g - \bar{h}) \Delta \rho - \dot{s} \rho C_p \nabla T \Delta t - \dot{m}_g'' C_{pg} \nabla T \Delta t \quad (\text{A4})$$

The internal energy at the next increment (U) can be obtained using the obtained ΔU as follows

$$U(t + \Delta T) = U(t) + \Delta U \quad (\text{A5})$$

$\partial U / \partial T$ and $\partial U / \partial \mathbf{g}$ can be obtained from Eq. (A4).

$$\frac{\partial U}{\partial T} = \rho C_p \quad (\text{A6})$$

$$\frac{\partial U}{\partial \mathbf{g}} = -\dot{s} \rho C_p \Delta t - \dot{m}_g'' C_{pg} \Delta t \quad (\text{A7})$$

From Eq. (A3), $\partial \mathbf{f} / \partial T$ and $\partial \mathbf{f} / \partial \mathbf{g}$ are obtained as follows.

$$\frac{\partial \mathbf{f}}{\partial T} = 0 \quad (\text{A8})$$

$$\frac{\partial \mathbf{f}}{\partial \mathbf{g}} = -k \quad (\text{A9})$$

In the case of the in-depth gas diffusion equation (Eq.(17)), it can be separated as follows. P is pressure, which is deemed as temperature.

Table A1 Six values for UMATHT

Internal energy (U)-related values			Flux (f)-related values		
U	$\partial U / \partial T$	$\partial U / \partial \mathbf{g}$	f	$\partial f / \partial T$	$\partial f / \partial \mathbf{g}$

$$\dot{U} = -\frac{\partial \rho}{\partial t} \quad (\text{A10})$$

$$\mathbf{f} = -\frac{\rho_g \kappa}{\mu \phi} \nabla P \quad (\text{A11})$$

As in the case of in-depth heat transfer, six values to be entered into UMATHT can be extracted from Eq. (A 10) and Eq. (A11). The three values related to the internal energy are as follows (Eqs. A12- A14).

$$\Delta U = -\Delta \rho \quad (\text{A12})$$

$$\frac{\partial U}{\partial P} = 0 \quad (\text{A13})$$

$$\frac{\partial U}{\partial \mathbf{g}} = 0 \quad (\text{A14})$$

If the pyrolysis gas is assumed to be an ideal gas, the gas's density can be expressed as Eq. (A.15).

$$\rho_g = \frac{PM_g}{RT} \quad (\text{A15})$$

With Eq. (A11) and Eq. (A15), values about flux (\mathbf{f}) are calculated.

$$\frac{\partial \mathbf{f}}{\partial P} = -\frac{M_g \kappa}{RT \mu \phi} \nabla P \quad (\text{A16})$$

$$\frac{\partial \mathbf{f}}{\partial \mathbf{g}} = -\frac{\rho_g \kappa}{\mu \phi} \quad (\text{A17})$$